

Universal set of quantum gates for the flip-flop qubit in the presence of 1/f noise

Elena Ferraro,^{1,*} Davide Rei,^{2,1} Matteo Paris,² and Marco De Michielis^{1,†}

¹*CNR-IMM Agrate Unit, Via C. Olivetti 2, 20864 Agrate Brianza (MB), Italy*

²*Quantum Technology Lab, Dipartimento di Fisica "Aldo Pontremoli", Università degli Studi di Milano, Via G. Celoria 16, 20133 Milano, Italy*

Impurities hosted in semiconducting solid matrices represent an extensively studied platform for quantum computing applications. In this scenario, the so-called flip-flop qubit emerges as a convenient choice for scalable implementations in silicon. Flip-flop qubits are realized implanting phosphorous donor in isotopically purified silicon, and encoding the logical states in the donor nuclear spin and in its bound electron. Electrically modulating the hyperfine interaction by applying a vertical electric field causes an Electron Dipole Spin Resonance (EDSR) transition between the states with antiparallel spins $\{|\downarrow\uparrow\rangle, |\uparrow\downarrow\rangle\}$, that are chosen as the logical states. When two qubits are considered, the dipole-dipole interaction is exploited allowing long-range coupling between them. A universal set of quantum gates for flip-flop qubits is here proposed and the effect of a realistic 1/f noise on the gate fidelity is investigated for the single qubit $R_z(-\frac{\pi}{2})$ and Hadamard gate and for the two-qubit \sqrt{iSWAP} gate.

I. INTRODUCTION

Quantum computing applications encompass a variety of different scientific, social and economical contexts, from fundamental science to finance, security and medical sectors. In the variegated landscape of physical qubits, semiconducting qubits encoding quantum information in the spin of electrons or nuclei confined through artificial atoms, such as quantum dots and donor atoms, are an established powerful tool [1–6]. In particular, donor spins have unprecedented advantages in terms of their long coherence time, high control and scalability. When a phosphorus donor is implanted in silicon, eventually using isotopically purified nanostructures (^{28}Si) to drastically reduce magnetic noise, another advantage comes out, that is the integrability with the Complementary Metal-Oxide-Semiconductor (CMOS) technology for the qubit fabrication [7].

The main obstacle to the realization of a donor-based quantum processor following Kane's seminal proposal [8] is the use a short-range interaction (10–15 nm) among qubits, namely the exchange interaction between the donor bound electrons, that requires a strong near-atomic precision in the donor implantation. One way to get around this issue, relaxing the strict requirement on donor placement, is based on the possibility to access long-range electric dipole-dipole interaction, thus reaching qubit distance up to hundreds of nm. In Ref. [9], a qubit in which an electric dipole is created sharing the electron between the donor and the interface has been proposed and called *flip-flop* qubit [10–13]. This qubit is manipulated by microwave electric field that modulates the hyperfine interaction. In addition, a dc electric field is applied to perform qubit rotations along the \hat{z} -axis of the Bloch sphere, and an ac electric field is required to

perform \hat{x} and \hat{y} rotations. The electrical control clearly makes the flip-flop qubit more sensitive to charge noise, that typically shows a 1/f spectrum, representing a not negligible source of decoherence [14].

In this paper, we present a universal set of quantum gates for quantum computation with flip-flop qubits. It is composed by the $R_z(-\frac{\pi}{2})$ and the Hadamard (H) one-qubit gates and the \sqrt{iSWAP} two-qubit gate. It is indeed possible to demonstrate that a universal gate set is $G = \{H, \Lambda(S)\}$, where $\Lambda(S)$ is a two-qubit gate in which the operation S is applied to the target qubit if and only if the control qubit is in the logical state $|1\rangle$, for example the CNOT gate [15]. Moreover, a construction of the CNOT gate using only $R_z(-\frac{\pi}{2})$, H and \sqrt{iSWAP} gates is feasible [16]. For each gate operation, we consider the effect of the charge noise using the 1/f model for the power spectral density.

The paper is organized as follows. In Section II we present the flip-flop qubit, its Hamiltonian model and the study on the noise effects on the fidelity for the single-qubit gates. In Section III we focus on the description of two interacting flip-flop qubits including the dipole-dipole interaction in the Hamiltonian model and then showing a fidelity analysis on the \sqrt{iSWAP} two-qubit gate. Section IV contains the main conclusions.

II. FLIP-FLOP QUBIT

The flip-flop qubit is realized embedding a phosphorous ^{31}P donor atom in a ^{28}Si nanostructure at a depth d from the interface (SiO_2 layer) as shown in Fig. 1

* elena.ferraro@mdm.imm.cnr.it

† marco.demichelis@mdm.imm.cnr.it

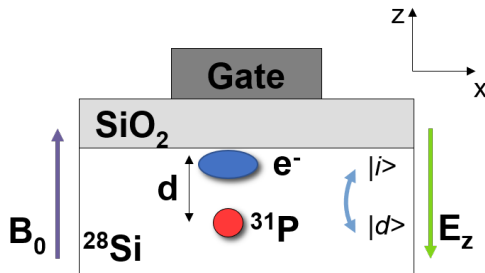


Figure 1. Scheme of the flip-flop qubit. A donor atom of ^{31}P is embedded in a bulk of ^{28}Si at a distance d from the Si/SiO_2 interface. The metal gate controls through an electric field E_z the electron position between the nucleus ($|d\rangle$) and the interface ($|i\rangle$) with the dielectric. A constant magnetic field B_0 is also applied.

A vertical electric field E_z applied by a metal gate on top, controls the position of the electronic wavefunction [9, 10]. The electronic spin ($S=1/2$) is described in the basis $\{| \downarrow \rangle, | \uparrow \rangle\}$ and has a gyromagnetic ratio $\gamma_e = 27.97$ GHz T^{-1} , while for the nuclear spin ($I=1/2$) the basis is denoted by $\{| \downarrow \rangle, | \uparrow \rangle\}$ and the gyromagnetic ratio is $\gamma_n = 17.23$ MHz T^{-1} , they interact through the hyperfine coupling A . Applying a large static magnetic field B_0 , (i.e. $(\gamma_e + \gamma_n)B_0 \gg A$), the eigenstates of the system are the four qubit states: $\{| \downarrow \uparrow \rangle, | \downarrow \downarrow \rangle, | \uparrow \downarrow \rangle, | \uparrow \uparrow \rangle\}$. Electrically modulating the hyperfine interaction A by E_z causes an Electron Dipole Spin Resonance (EDSR) transition between the states with antiparallel spins $\{| \downarrow \uparrow \rangle, | \uparrow \downarrow \rangle\}$, that are in turn chosen to encode the qubit.

A. Hamiltonian model

The flip-flop qubit Hamiltonian model H^{ff} is given by the sum of three contributions [9, 12]

$$H^{ff} = H_{orb} + H_{B_0} + H_A. \quad (1)$$

The first term is the orbital Hamiltonian that reads (in units of Hz):

$$H_{orb} = -\frac{\varepsilon_0}{2}\sigma_z - \frac{deE_{ac}(t)}{2h} \left(\frac{de\Delta E_z}{h\varepsilon_0}\sigma_z + \frac{V_t}{\varepsilon_0}\sigma_x \right), \quad (2)$$

where V_t is the tunnel coupling between the donor and the interface potential wells; $\Delta E_z = E_z - E_z^0$ where E_z^0 is the vertical electric field at the ionization point, i.e. the point in which the electron is shared halfway between the donor and the interface; $\varepsilon_0 = \sqrt{V_t^2 + (de\Delta E_z/h)^2}$ is the energy difference between the orbital eigenstates, where h is the Planck's constant, d is the distance from the interface, hereafter $d=15$ nm, and e is the elementary charge. For completeness, the ac electric field $E_{ac}(t)$ is also included and is equal to $E_{ac} \cos(\omega_E t + \phi)$. It is applied in resonance with the flip-flop qubit, i.e. $\omega_E = 2\pi\epsilon_{ff}$, where ϵ_{ff} is the flip-flop qubit transition frequency, and ϕ is an

additional phase. The Pauli matrices are expressed in the basis of the orbital eigenstates: $\sigma_z = |g\rangle\langle g| - |e\rangle\langle e|$ and $\sigma_x = |g\rangle\langle e| + |e\rangle\langle g|$, where $|g\rangle$ ($|e\rangle$) is the ground (excited) state of the orbital part of the Hamiltonian. We point out that the electron position operators, i.e. $\sigma_z^{id} = |i\rangle\langle i| - |d\rangle\langle d|$ and $\sigma_x^{id} = |i\rangle\langle d| + |d\rangle\langle i|$, where $|i\rangle$ ($|d\rangle$) denotes the interface (donor) electron position, are expressed in the orbital eigenbasis, by the following relation: $\sigma_z^{id} = \frac{de\Delta E_z}{h\varepsilon_0}\sigma_z + \frac{V_t}{\varepsilon_0}\sigma_x$ and $\sigma_x^{id} = -\frac{V_t}{\varepsilon_0}\sigma_z + \frac{de\Delta E_z}{h\varepsilon_0}\sigma_x$.

The second term in Eq.(1) is the Zeeman interaction due to the presence of the static magnetic field B_0 oriented along the \hat{z} axis and includes also the dependence of the electron Zeeman splitting on its orbital position through the quantity Δ_γ (that in the following we set to -0.2%). The Zeeman term H_{B_0} may be written

$$H_{B_0} = \gamma_e B_0 \left[\mathbb{1} + \left(\frac{1}{2} + \frac{de\Delta E_z}{2h\varepsilon_0}\sigma_z + \frac{V_t}{2\varepsilon_0}\sigma_x \right) \Delta_\gamma \right] S_z - \gamma_n B_0 I_z, \quad (3)$$

where $\mathbb{1}$ is the identity operator on the orbital subspace and $B_0=0.4$ T.

Finally, the hyperfine interaction is given by

$$H_A = A(\Delta E_z) \left(\frac{1}{2} - \frac{de\Delta E_z}{2h\varepsilon_0}\sigma_z - \frac{V_t}{2\varepsilon_0}\sigma_x \right) \mathbf{S} \cdot \mathbf{I}, \quad (4)$$

where the dependence of the hyperfine coupling A by the electric field is highlighted. To obtain the functional form of $A(\Delta E_z)$, that changes from the bulk value $A_0=117$ MHz to 0 when the electron is at the interface, we fit the results from Ref.[9] with the function $A_0/(1 + e^{c\Delta E_z})$, obtaining $c = 5.174 \cdot 10^{-4}$ m/V.

We assume a qubit working temperature of $T=100$ mK, so as to ensure that the thermal energy $k_B T$ (where k_B is the Boltzmann constant) is always lower than the minimum qubit energy $\epsilon_{ff} = \sqrt{(\gamma_e + \gamma_n)^2 B_0^2 + A(E_z)^2}$, that is $\simeq 11$ GHz.

We chose to describe the flip-flop qubit expressing its Hamiltonian in the complete eight-dimensional basis $\{|g\downarrow\uparrow\rangle, |g\downarrow\downarrow\rangle, |e\downarrow\uparrow\rangle, |g\uparrow\uparrow\rangle, |g\uparrow\downarrow\rangle, |e\downarrow\downarrow\rangle, |e\uparrow\uparrow\rangle, |e\uparrow\downarrow\rangle\}$, where the states are ordered from the lower to the higher corresponding energy values, and $\{|g\downarrow\uparrow\rangle, |g\uparrow\downarrow\rangle\}$ are respectively the $\{|0\rangle, |1\rangle\}$ logical states.

B. Single-qubit gates

In this subsection we present the results obtained analyzing the entanglement fidelity for the single-qubit $R_z(-\frac{\pi}{2})$ and H gates when the 1/f noise model is included [14, 17–20]. The 1/f noise model is based on the definition of the Power Spectral Density (PSD) that is inversely proportional to the frequency and is given by $S(\omega) = \alpha/(\omega t_0)$, where α is the noise amplitude, that

does not depend on ω and t_0 is the time unit. Following Ref. [21] we generated the 1/f noise in the frequency domain as

$$n(\omega) = m(\omega)^{-1/2} e^{i\varphi(\omega)}, \quad (5)$$

where $m(\omega)$ is generated from a standard Gaussian white process and the phase factor $\varphi(\omega) = [0, 2\pi]$ is chosen uniformly. To obtain the noise in the time domain, we calculate the inverse Fourier transform and then multiply the result by the noise amplitude α .

1. $R_z(-\frac{\pi}{2})$ gate

The rotation of an angle $-\pi/2$ around the \hat{z} -axis of the Bloch sphere is obtained in the following way: a dc elec-

tric field $\Delta E_z(t)$ is adiabatically swept to move the electron from the interface at an idling electric field ΔE_{idle} to the value of clock transition (CT) ΔE_{ct} , and back. The adiabatic set-up consists of a first fast step of duration τ_1 , reaching an intermediate value ΔE_{int} , and a second slower step of duration τ_2 reaching ΔE_{ct} . Then, the electron remains at the CT for a time T before coming back at the idling. The ac electric field is zero. In Table I all the parameters set to implement the $R_z(-\frac{\pi}{2})$ gate are reported, T_{gate} denotes the total gate time.

Table I. $R_z(-\frac{\pi}{2})$ gate parameters

ΔE_{idle} [V/m]	ΔE_{int} [V/m]	ΔE_{ct} [V/m]	τ_1 [ns]	τ_2 [ns]	T [ns]	V_t [GHz]	K	T_{gate} [ns]
10000	500	290	1.7	3.5	21.6	11.29	$\simeq 20$	31.9

The coefficient K , representing the adiabatic factor, is calculated as the minimum value between the charge adiabatic factor K_c and the spin-orbit adiabatic factor K_{so} . Both are derived from a simple two-level Hamiltonian model [9]

$$H = \Delta\sigma_z + \Omega\sigma_x \quad (6)$$

and the adiabatic condition holds when

$$K = \left| \frac{\omega_{eff}}{\dot{\beta}} \right| \gg 1, \quad (7)$$

where $\omega_{eff} = \sqrt{\Delta^2 + \Omega^2}$ and $\beta = \arctan(\frac{\Omega}{\Delta})$. For the $R_z(-\frac{\pi}{2})$ gate, in order to find K_c for the charge qubit, we use $\Delta_c = \frac{\pi e d \Delta E_z}{\hbar}$ and $\Omega_c = \pi V_t$, whereas for the spin-charge coupling we use $\Delta_{so} = \pi \delta_{so}$, where $\delta_{so} = \varepsilon_0 - \varepsilon_{ff}$ with $\varepsilon_{ff} = \sqrt{(\gamma_e + \gamma_n)^2 B_0^2 + A(\Delta E_z)^2}$, that is the flip-

flop qubit transition frequency, and $\Omega_{so} = 2\pi g_{so}$ where $g_{so} = \frac{A}{4} \frac{V_t}{\varepsilon_0}$.

In Fig. 2(a) we report the dynamical behaviour of the dc field $\Delta E_z(t)$ as well as the mean values of the single qubit operators: $\sigma_z^{ff} = |\uparrow\downarrow\rangle\langle\uparrow\downarrow| - |\downarrow\uparrow\rangle\langle\downarrow\uparrow|$, $\sigma_x^{ff} = |+_{x^f}^{ff}\rangle\langle+_{x^f}^{ff}| - |-_{x^f}^{ff}\rangle\langle-_{x^f}^{ff}|$ with $|\pm_x^{ff}\rangle = (|\uparrow\downarrow\rangle \pm e^{-i2\pi\varepsilon_{ff}^{t=0}} |\downarrow\uparrow\rangle)/\sqrt{2}$, σ_z^{id} and the charge excitation $|e\rangle\langle e|$ in the flip-flop subspace during the evolution of the $R_z(-\frac{\pi}{2})$ gate. To provide an example, we have chosen to start from the initial condition $|\psi_0\rangle = \frac{|0\rangle + |1\rangle}{\sqrt{2}}$. Fig. 2(b) shows the Bloch sphere representation of the $R_z(-\frac{\pi}{2})$ gate operation when the qubit is observed in the laboratory frame (left) and in a frame rotating at the angular frequency of an idling qubit (right). The yellow arrow represents the expected final state obtained after the application of the sequence.

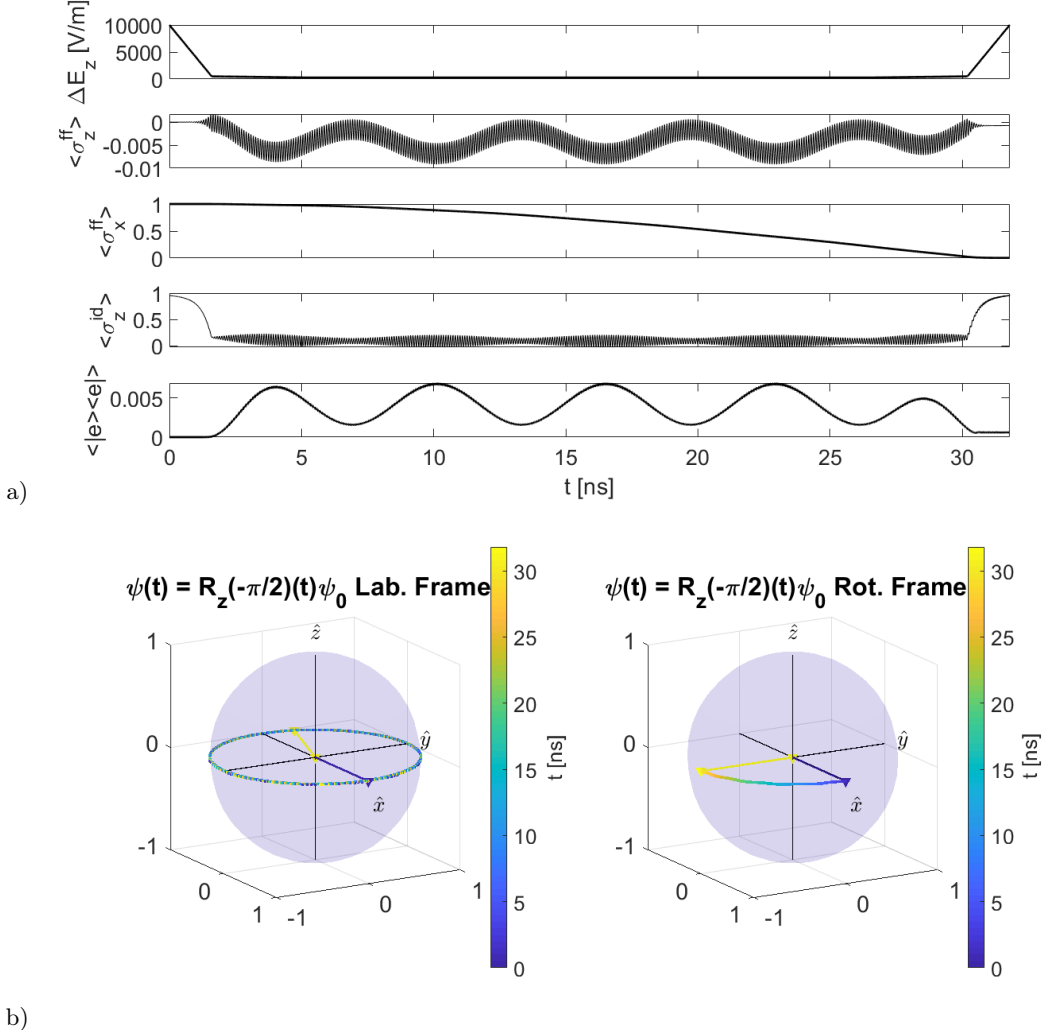


Figure 2. (a) Time evolution of the dc applied electric field $\Delta E_z(t)$ and of the mean values of the operators σ_z^{ff} , σ_x^{ff} , σ_z^{id} and $|e\rangle\langle e|$ during the evolution of the $R_z(-\frac{\pi}{2})$ gate for the initial state $|\psi_0\rangle = \frac{|0\rangle+|1\rangle}{\sqrt{2}}$. (b) Bloch sphere representation of the $R_z(-\frac{\pi}{2})$ gate. The blue (yellow) arrow represents the initial (final) state in the laboratory frame (left) and in the rotating frame (right).

2. Hadamard gate

The Hadamard gate acts on the qubit as a rotation of an angle π around the $(\hat{x} + \hat{z})/\sqrt{2}$ axis. It is obtained by applying both the dc and the ac electric fields. The dc electric field is applied following the procedure described

before for the $R_z(-\frac{\pi}{2})$ gate. In addition, when $\Delta E_z(t) = \Delta E_{ct}$ an ac electric field $E_{ac}(t)$ in resonance with the flip-flop transition frequency is applied for a time $T_{E_{ac}}^{ON}$ with $\phi = -\pi/2$. In Table II all the parameters set to implement the H gate are reported.

Table II. H gate parameters

ΔE_{idle} [V/m]	ΔE_{int} [V/m]	ΔE_{ct} [V/m]	E_{ac} [V/m]	τ_1 [ns]	τ_2 [ns]	T [ns]	$T_{E_{ac}}^{ON}$ [ns]	V_t [GHz]	K	K_E	T_{gate} [ns]
10000	500	0	180	1.7	3.5	41.5	40	11.5	$\simeq 21$	$\simeq 57$	51.9

For the H gate, in addition to the adiabaticity factor K , we evaluated K_E using $\Delta_E = \pi\delta_E$ where $\delta_E = \omega_E/(2\pi) - \varepsilon_0$ and $\Omega_E = 2\pi g_E$ where $g_E = \frac{edE_{ac}}{4\hbar} \frac{V_t}{\varepsilon_0}$.

Analogously to the $R_z(-\frac{\pi}{2})$ gate, in Fig. 3 we observe the behavior of the H gate starting from the qubit initial condition $|\psi_0\rangle = |0\rangle$.

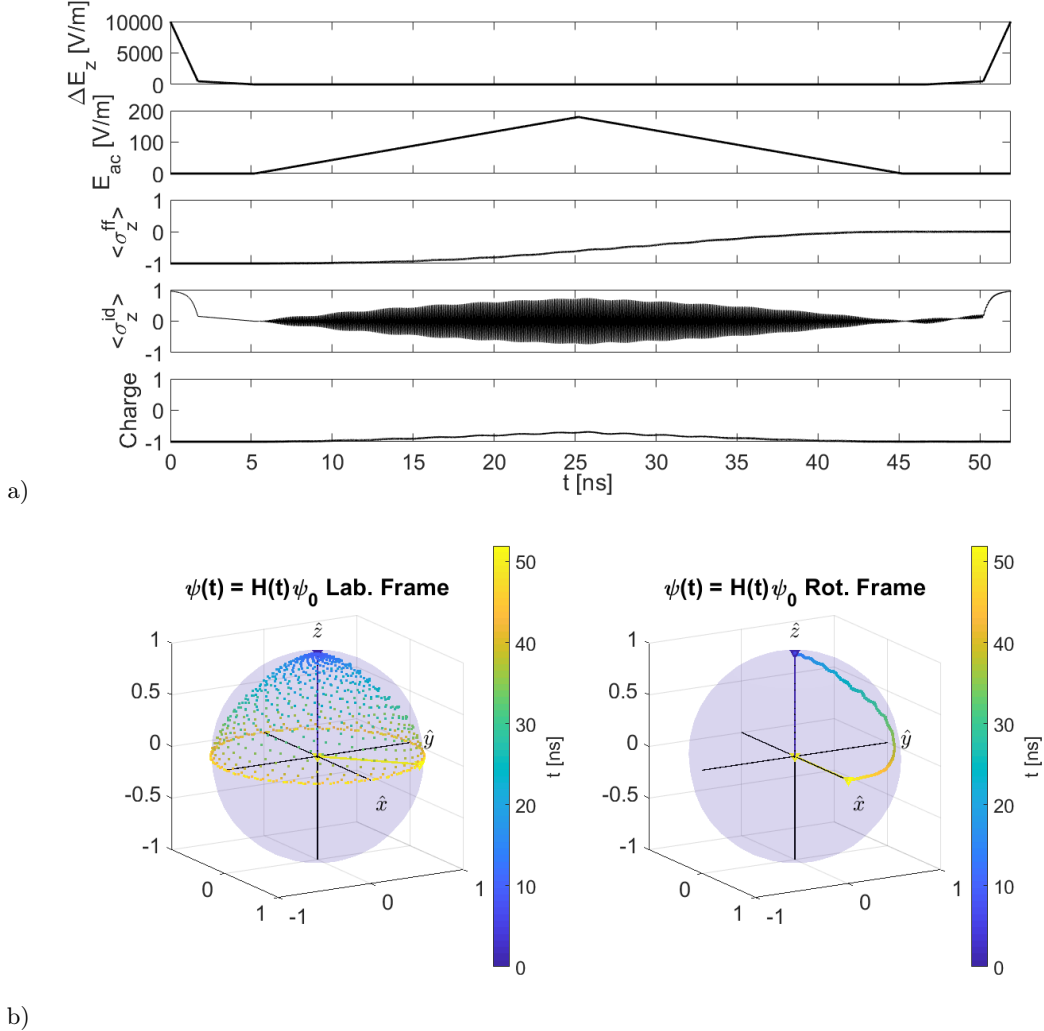


Figure 3. (a) Time evolution of the dc applied electric field $\Delta E_z(t)$, of the amplitude of the ac electric field $E_{ac}(t)$ and of the mean values of the operators σ_z^{ff} , σ_z^{id} and the charge operator $|e\rangle \langle e| - |g\rangle \langle g|$ in the flip-flop subspace during the evolution of the H gate for the initial state $|\psi_0\rangle = |0\rangle$. (b) Bloch sphere representation of the H gate. The blue (yellow) arrow represents the initial (final) state in the laboratory frame (left) and in the rotating frame (right).

3. Entanglement fidelity

In order to assess the performance of our gates in the presence of noise, we adopt the entanglement fidelity F [22, 23], that does not depend on the qubit initial condition, and is defined as

$$F = \text{tr}[\rho^{RS} \mathbb{1}_R \otimes (U_i^{-1} U_d)_S \rho^{RS} \mathbb{1}_R \otimes (U_d^{-1} U_i)_S], \quad (8)$$

where U_d (U_i) is the disturbed (ideal) quantum gate and $\rho^{RS} = |\psi\rangle \langle \psi|$ where $|\psi\rangle$ represents a maximally entan-

gled state in a double state space generated by two identical Hilbert spaces R and S , that is $|\psi\rangle = \frac{1}{\sqrt{2}}(|00\rangle + |11\rangle)$ for the single qubit gates and $|\psi\rangle = \frac{1}{\sqrt{2}}(|0000\rangle + |1111\rangle)$ for the two-qubit gate.

In Fig. 4 we show the entanglement infidelity $1-F$ for the $R_z(-\frac{\pi}{2})$ and the H gates when a noise amplitude $\alpha_{\Delta E_z}$ on the electric field ΔE_z in the interval $[1, 1000]$ V/m is considered.

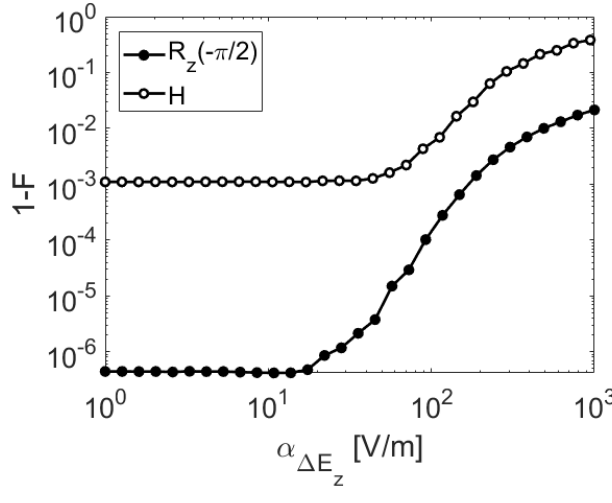


Figure 4. Entanglement infidelity for the $R_z(-\frac{\pi}{2})$ and H gates as a function of the noise amplitude $\alpha_{\Delta E_z}$.

For both the quantum gates we observe the same qualitative behaviour of the infidelity. In the intervals $\alpha_{\Delta E_z} \simeq [1, 20]$ V/m for $R_z(-\frac{\pi}{2})$ and $\alpha_{\Delta E_z} \simeq [1, 40]$ V/m for H, the infidelities show a plateau that reflects the non-adiabaticity of the sequence. Increasing the value of the coefficient K leads to a more adiabatic operation that returns a lower value of the infidelities in the plateau. In this region, the $R_z(-\frac{\pi}{2})$ gate shows the higher values of fidelity, that is, around 99.9999%, followed by the H gate fidelity that starts approximately from 99.9%. Then the infidelities slowly grow up until they settle to higher values in correspondence to high values of the noise amplitude. For all the gates under study, the fidelities show very promising values up to very reasonable values of the experimental noise amplitude, i.e. $\alpha_{\Delta E_z} \leq 100$ V/m. Indeed, we have $F \geq 99.99\%$ for the $R_z(-\frac{\pi}{2})$ gate and $F \geq 99.3\%$ for the H gate.

III. TWO FLIP-FLOP QUBITS

The universal set of quantum gates may be completed by the \sqrt{iSWAP} two-qubit gate. In the first part of this

Section, we present the Hamiltonian model describing two interacting flip-flop qubits, whereas in the second part the \sqrt{iSWAP} is derived and the effects of the noise are investigated.

A. Hamiltonian model

The two flip-flop qubits Hamiltonian model H^{2ff} is obtained adding up two single-qubit Hamiltonians, supposed identical, and an interaction term

$$H^{2ff} = H^{ff} \otimes \mathbb{1} + \mathbb{1} \otimes H^{ff} + H_{int}. \quad (9)$$

H_{int} is the dipole-dipole interaction and is equal to

$$H_{int} = \frac{1}{4\pi\epsilon_0\epsilon_r r^3} \left[\mathbf{p}_1 \cdot \mathbf{p}_2 - \frac{3(\mathbf{p}_1 \cdot \mathbf{r})(\mathbf{p}_2 \cdot \mathbf{r})}{r^2} \right], \quad (10)$$

where ϵ_0 (ϵ_r) is the vacuum permittivity (material dielectric constant, that we set to the silicon value 11.7) and \mathbf{r} is the two-qubit distance. The dipole operator is $p_k = de(\mathbb{1} + \sigma_{z,k}^{id})/2$, ($k = 1, 2$), and we assume that the dipoles are oriented perpendicularly to their separation, i.e. $\mathbf{p}_k \cdot \mathbf{r} = 0$. From all these considerations, we have

$$H_{int} = \frac{d^2 e^2}{16\pi\epsilon_0\epsilon_r h r^3} (\mathbb{1}_1 \mathbb{1}_2 + \sigma_{z,1}^{id} \mathbb{1}_2 + \mathbb{1}_1 \sigma_{z,2}^{id} + \sigma_{z,1}^{id} \sigma_{z,2}^{id}). \quad (11)$$

B. Two-qubit gate: \sqrt{iSWAP}

The matrix that represents the \sqrt{iSWAP} gate in the two-qubit logical basis is given by

$$\sqrt{iSWAP} = \begin{pmatrix} 1 & 0 & 0 & 0 \\ 0 & \frac{1}{\sqrt{2}} & \frac{1}{\sqrt{2}}i & 0 \\ 0 & \frac{1}{\sqrt{2}}i & \frac{1}{\sqrt{2}} & 0 \\ 0 & 0 & 0 & 1 \end{pmatrix} \quad (12)$$

and the set of parameters included into the sequence that realize the transformation in Eq.(12) is reported in Table III.

Table III. \sqrt{iSWAP} gate parameters

ΔE_{idle} [V/m]	ΔE_{int} [V/m]	ΔE_{ct} [V/m]	τ_1 [ns]	τ_2 [ns]	T [ns]	V_t [GHz]	K	T_{gate} [ns]
Q_1Q_2	10000	500	0	1.7	99	2	11.58	$\simeq 21$
$Q_1(Q_2)$	10000	500	0	1.7	3.5	1.2	11.58	$\simeq 21$

The operation is obtained by first applying to both

the qubits Q_1Q_2 a dc electric field $\Delta E_z(t)$ with $\tau_1 = 1.7$

ns, $\tau_2=99$ ns and $T=2$ ns, and then by applying two identical single qubit rotations to Q_1 and later to Q_2 along the \hat{z} axis with $\tau_1=1.7$ ns, $\tau_2=3.5$ ns and $T=1.2$ ns, that corresponds to a rotation angle $\theta \simeq -0.5$ rad. When Q_1 performs the \hat{z} -rotation, Q_2 is in ΔE_{idle} , and viceversa. The total time to perform the \sqrt{iSWAP} is given by $T_{gate} = T_{gate}^{Q_1Q_2} + T_{gate}^{Q_1} + T_{gate}^{Q_2} = 226.6$ ns.

The dynamical behaviour of the two electric fields $\Delta E_{z,1}(t)$ and $\Delta E_{z,2}(t)$ applied respectively to Q_1 and to Q_2 are shown in Fig. 5(a). In addition, the mean values of the operators for both the qubits are shown. In Fig. 5(b) we report the dynamical behaviour on the Bloch sphere during the application of the entire sequence for Q_1 (left) and Q_2 (right) in the rotating frame, starting from the initial condition $|\psi_0\rangle = |\psi_{01}\rangle \otimes |\psi_{02}\rangle$ with $|\psi_{01}\rangle = |1\rangle$ for Q_1 and $|\psi_{02}\rangle = |0\rangle$ for Q_2 .

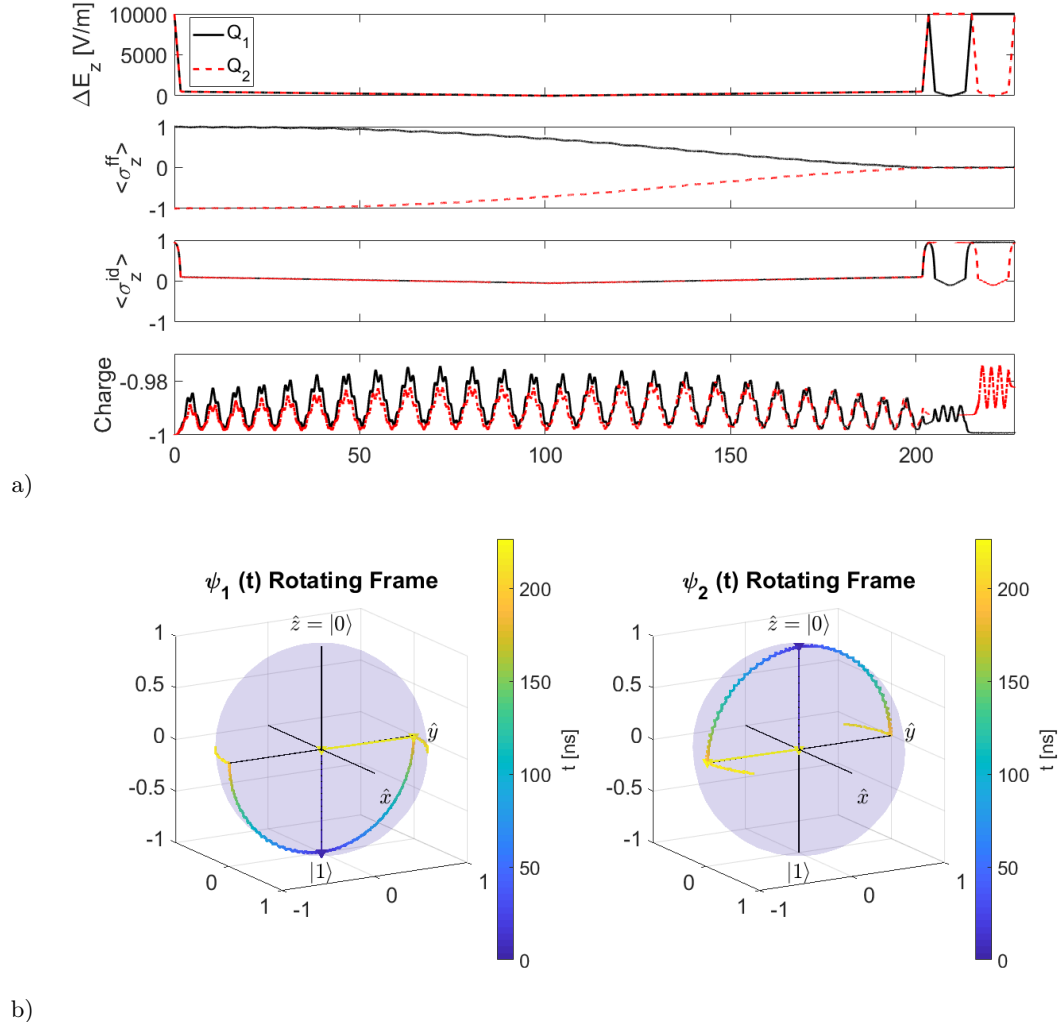


Figure 5. (a) Time evolution of the dc applied electric fields $\Delta E_{z,1}(t)$ and $\Delta E_{z,2}(t)$ and of the mean values of the operators $\sigma_{z,(1,2)}^{ff}$, $\sigma_{z,(1,2)}^{id}$ and the charge operator $|e\rangle\langle e| - |g\rangle\langle g|$ for the two flip-flop qubits during the evolution of the \sqrt{iSWAP} gate for the initial state $|\psi_0\rangle = |\psi_{01}\rangle \otimes |\psi_{02}\rangle$ with $|\psi_{01}\rangle = |1\rangle$ and $|\psi_{02}\rangle = |0\rangle$. (b) Bloch sphere representation of the \sqrt{iSWAP} gate. The blue (yellow) arrow represents the initial (final) state for Q_1 (left) and Q_2 (right) in the rotating frame.

In Fig. 6 we report the entanglement infidelity for the \sqrt{iSWAP} gate when a noise amplitude $\alpha_{\Delta E_z}$ in the interval $[1, 1000]$ V/m is considered.

When the noise amplitude lies in the interval $[1, 10]$

V/m, the fidelity is $F \simeq 99.98\%$ and it remains larger than $F \simeq 99.5\%$ up to $\alpha_{\Delta E_z} \simeq 50$ V/m.

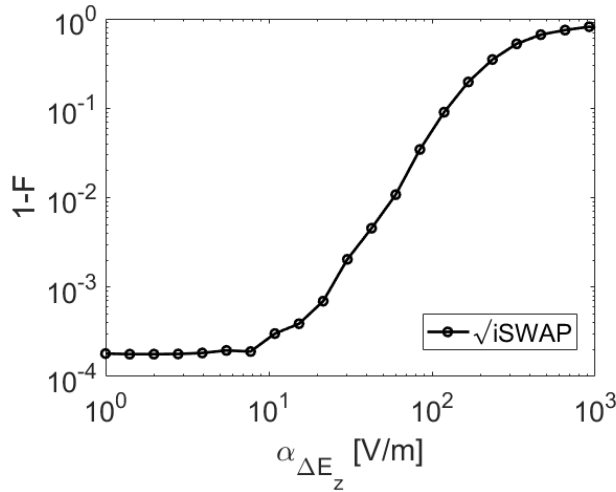


Figure 6. Entanglement infidelity for the \sqrt{iSWAP} gate as a function of the noise amplitude $\alpha_{\Delta E_z}$.

IV. CONCLUSIONS

In this paper we have addressed quantum computation by flip-flop qubits, a donor-based qubits in which the logical states are encoded in the donor nuclear and its bound electron. Flip-flop qubits represent an interesting advancement compared to the Kane's seminal proposal, due to the possibility of exploiting the long range electric dipole-dipole interaction. A universal set of quantum gates composed by $\{R_z(-\frac{\pi}{2}), H, \sqrt{iSWAP}\}$ has been presented, and the noise effect on the entanglement fidelity has been studied. The noise model adopted shows a $1/f$ spectrum, typical of qubits sensitive to charge noise. In terms of fidelity, results are very promising: for example in correspondence to a realistic noise level around 50 V/m, we obtain $F \geq 99.999\%$ for the $R_z(-\frac{\pi}{2})$ gate and 99.8% for the H gate. Under the same condition, the two-qubit \sqrt{iSWAP} gate may be realized with a fidelity above 99.5%. We conclude that flip-flop qubits with long range coupling represent a promising platform for solid state quantum computation.

[1] J. J. L. Morton, D. R. McCamey, M. A. Eriksson, and S. A. Lyon, *Nature* **479**, 345 (2011).

[2] A. Laucht, J. T. Muhonen, F. A. Mohiyaddin, R. Kalra, J. P. Dehollain, S. Freer, F. E. Hudson, M. Veldhorst, R. Rahman, G. Klimeck, K. M. Itoh, D. N. Jamieson, J. C. McCallum, A. S. Dzurak, and A. Morello, *Science Advances* **1**, e1500022 (2015).

[3] M. Veldhorst, H. Eenink, C. Yang, and A. Dzurak, *Nature Communications* **8**, 1766 (2017).

[4] L. M. K. Vandersypen, H. Bluhm, J. S. Clarke, A. S. Dzurak, R. Ishihara, A. Morello, D. J. Reilly, L. R. Schreiber, and M. Veldhorst, *Npj Quantum Information* **3**, 34 (2017).

[5] K. W. Chan, W. Huang, C. H. Yang, J. C. C. Hwang, B. Hensen, T. Tanttu, F. E. Hudson, K. M. Itoh, A. Laucht, A. Morello, and A. S. Dzurak, *Physical Review Applied* **10**, 044017 (2018).

[6] C. H. Yang, R. C. C. Leon, J. C. C. Hwang, A. Saraiva, T. Tanttu, W. Huang, J. C. Lemyre, K. W. Chan, K. Y. Tan, F. E. Hudson, K. M. Itoh, A. Morello, M. Pioro-Ladrière, A. Laucht, and A. S. Dzurak, *Nature* **580**, 350 (2020).

[7] R. Maurand, X. Jehl, D. Kotekar-Patil, A. Corna, H. Boushavskyi, R. Laviéville, L. Hutin, S. Barraud, M. Vinet, M. Sanquer, *et al.*, *Nature Communications* **7**, 13575 (2016).

[8] B. E. Kane, *Nature* **393**, 133 (1998).

[9] G. Tosi, F. A. Mohiyaddin, V. Schmitt, S. Tenberg, R. Rahman, G. Klimeck, and A. Morello, *Nature Communications* **8**, 450 (2017).

[10] G. Tosi, F. A. Mohiyaddin, S. Tenberg, A. Laucht, and A. Morello, *Physical Review B* **98**, 075313 (2018).

[11] P. Boross, G. Széchenyi, and A. Pályi, *Nanotechnology* **27**, 314002 (2016).

[12] J. Simon, F. A. Calderon-Vargas, E. Barnes, and S. E. Economou, *Physical Review B* **101**, 205307 (2020).

[13] F. A. Calderon-Vargas, E. Barnes, and S. E. Economou, *arXiv:2101.11592v1* (2021).

[14] E. Paladino, Y. M. Galperin, G. Falci, and B. L. Altshuler, *Review of Modern Physics* **86**, 361 (2014).

[15] J. Preskill, *Lecture Notes for Ph219/CS219: Quantum Information and Computation* (2015).

[16] N. Schuch and J. Siewert, *Physical Review A* **67**, 032301 (2003).

[17] J. M. Epstein, A. W. Cross, E. Magesan, and J. M. Gambetta, *Physical Review A* **89**, 062321 (2014).

[18] C. Zhang, R. E. Throckmorton, X. C. Yang, X. Wang, E. Barnes, and S. DasSarma, *Physical Review Letters* **118**, 216802 (2017).

[19] Y.-C. Yang, S. N. Coppersmith, and M. Friesen, *Physical Review A* **100**, 022337 (2019).

[20] E. Ferraro and M. De Michielis, *Scientific Reports* **10**, 17780 (2020).

[21] X. Yang and X. Wang, *Scientific Reports* **6**, 28996 (2016).

[22] M. A. Nielsen and I. L. Chuang, *Quantum Computation and Quantum Information* (Cambridge University Press, Cambridge, 2000).

[23] D. C. Marinescu and G. M. Marinescu, *Classical and Quantum Information* (Elsevier, Amsterdam, 2012).